BIOCHEMISTRY
including biophysical chemistry & molecular biology

Article

pubs.acs.org/biochemistry

The Siderophore-Interacting Protein YqjH Acts as a Ferric Reductase in Different Iron Assimilation Pathways of *Escherichia coli*

Marcus Miethke,* Jie Hou, and Mohamed A. Marahiel

Department of Chemistry/Biochemistry, Philipps University Marburg, Hans Meerwein Strasse, D-35032 Marburg, Germany

Supporting Information

ABSTRACT: Siderophore-interacting proteins (SIPs), such as YqjH from *Escherichia coli*, are widespread among bacteria and commonly associated with iron-dependent induction and siderophore utilization. In this study, we show by detailed biochemical and genetic analyses the reaction mechanism by which the YqjH protein is able to catalyze the release of iron from a variety of iron chelators, including ferric triscatecholates and ferric dicitrate, displaying the highest efficiency for the hydrolyzed ferric enterobactin complex ferric (2,3-dihydroxybenzoylserine)$_3$. Site-directed mutagenesis revealed that residues K55 and R130 of YqjH are crucial for both substrate binding and reductase activity. The NADPH-dependent iron reduction was found to proceed via single-electron transfer in a double-displacement-type reaction through formation of a transient flavosemiquinone. The capacity to reduce substrates with extremely negative redox potentials, though at low catalytic rates, was studied by displacing the native FAD cofactor with 5-deaza-5-carba-FAD, which is restricted to a two-electron transfer. In the presence of the reconstituted noncatalytic protein, the ferric enterobactin midpoint potential increased remarkably and partially overlapped with the effective E_1 redox range. Concurrently, the observed molar ratios of generated Fe(II) versus NADPH were found to be ~1.5-fold higher for hydrolyzed ferric triscatecholates and ferric dicitrate than for ferric enterobactin. Further, combination of a chromosomal *yqjH* deletion with *entC* single- and *entC fes* double-deletion backgrounds showed the impact of *yqjH* on growth during supplementation with ferric siderophore substrates. Thus, YqjH enhances siderophore utilization in different iron acquisition pathways, including assimilation of low-potential ferric substrates that are not reduced by common cellular cofactors.

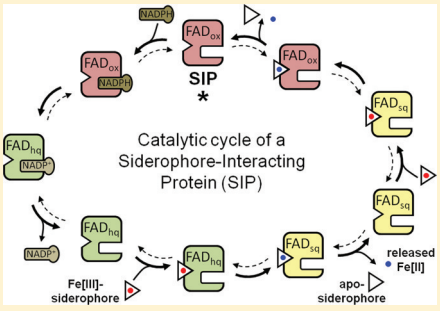

The efficient utilization of siderophores for iron assimilation under iron-limiting conditions is crucial for both pathogenic and nonpathogenic bacteria in various habitats. In particular, bacteria that colonize mammalian hosts are generally faced with strong iron deprivation because of the tight systemic iron homeostasis, and hence, their siderophores represent key factors for opportunistic growth or, in the case of pathogens, the development of virulence.[1,2]

Iron that is taken up by siderophores is released for further intracellular channeling either by partial hydrolysis of the siderophore scaffold or by reduction of the coordinated ferric iron species.[3] Ferric siderophore reduction has an advantage of reutilizing intact siderophores and, thus, saving substrate and energy cost for their de novo biosynthesis. However, the efficiency of reduction is largely dependent on the ferric siderophore redox potentials, which drastically vary over the range of different structural siderophore classes in combination with local proton activity and binding equilibria of oxidized and reduced species.[4,5]

One outstanding class of siderophores consists of the triscatecholates, because they provide the highest formation constants for ferric iron with log K_f values near 50 and, at the same time, $E^{\circ\prime}$ redox potentials for the free complexes as low as −750 mV.[6,7] Different variants of triscatecholates, including enterobactin, salmochelins, vibriobactin, and bacillibactin, are commonly produced by both predominantly nonpathogenic strains such as commensal variants of *Escherichia coli*[8] and various pathogens like *Salmonella enterica*,[9] *Vibrio cholerae*,[10] and *Bacillus anthracis* or *Bacillus cereus*,[11,12] respectively.

As a distinct structural feature, enterobactin, bacillibactin, and salmochelins possess trilactone backbones, making them readily available substrates for ester hydrolysis upon being imported into the cytosol. The intracellular trilactone hydrolases Fes,[13] IroD,[14,15] and BesA[16,17] are known to act specifically on the iron-charged complexes of these siderophores, and genetic analysis revealed the essentiality of these esterases during iron homeostasis.[15,16] However, the subsequent steps of release of iron from hydrolyzed ferric triscatecholate scaffolds is not fully understood. In the case of ferric enterobactin, the formation constants of its hydrolysis product as well as structurally similar ferric catecholate compounds are in a range that still favors complex formation rather than iron dissociation.[18,19] Furthermore, the midpoint potential (approximately −350 mV) of the free ferric (2,3-dihydroxybenzoylserine)$_3$ complex[6] is in a range comparable to that of intact ferric hydroxamate siderophores, which are known to require ferric reductase activities for efficient iron assimilation.[5,20] Reductive release is even more essential

Received: September 29, 2011
Revised: November 10, 2011
Published: November 18, 2011

ACS Publications © 2011 American Chemical Society

in cases of triscatecholates whose ferric complexes cannot be entropically affected by ester hydrolysis, such as vibriobactin and structural analogues, including fluvibactin, vulnibactin, agrobactin, parabactin, and protochelin.[21] These siderophores are produced by bacterial species that usually possess "siderophore-interacting proteins" (SIPs). One of the first SIPs was described as the ViuB protein in *V. cholerae*, which was found to be essential for ferric vibriobactin utilization and furthermore to complement the *E. coli* Fes esterase, although no hydrolytic activity was proposed for this component.[22] Crystallographic studies of ViuB homologues from *Shewanella putrefaciens* [Protein Data Bank (PDB) entry 2GPJ][23] and from *E. coli*[24] showed that these proteins are similar to members of the NAD(P)H:flavin oxidoreductase family, possessing a tightly bound FAD cofactor in the proximity of a potential substrate binding site. The ViuB homologue YqjH from *E. coli* was shown to be a Fur-regulated protein.[25,26] YqjH was further initially characterized with regard to its reductase activity, showing that ferric complexes could be reduced in the presence of NADPH as the preferred electron donor substrate.[26] Additionally, a nickel-dependent regulation of YqjH by the YqjI repressor was demonstrated, suggesting an association between YqjH-dependent iron utilization and the assembly of Fe- and Ni-containing proteins.[26]

In this study, we show by a detailed mechanistic analysis of the kinetic reaction type together with the elucidation of the efficient enzyme−substrate redox ranges that YqjH is in fact capable of catalyzing reductive iron release in a step that directly follows the trilactone backbone hydrolysis of ferric enterobactin. Further, we demonstrate that YqjH can also contribute to the reduction of ferric iron in complex with intact triscatecholates, and that it acts in further iron acquisition pathways such as that for ferric dicitrate. Our in vitro and in vivo results indicate that YqjH represents a redox factor that enhances the efficiency of ferric iron assimilation during siderophore-dependent iron homeostasis.

MATERIALS AND METHODS

Cloning and Expression. The *yqjH* gene from *E. coli* K12 was amplified from genomic DNA using primers 5′-ATATCTAGACACGAAGGCGATAACAATGAATAAC-3′ and 5′-ATAAGCGCTCTTTGCGTGCCAGTAAGCCGC-3′, containing *Xba*I and an *Eco*47III restriction sites (both underlined), respectively. The polymerase chain reaction (PCR) product was cloned into vector pMM30,[27] resulting in the pMM30-3 expression vector providing a $tet^{p/o}$ site and a C-terminal Strep-tag II translational fusion. DNA isolations, in vitro manipulations due to cloning, and transformations were conducted as previously described.[28] *E. coli* BL21 cells transformed with the expression vector were grown in LB medium at 37 °C until the OD_{600} reached 0.6 and then induced with 0.2 mg/L anhydrotetracycline for 4 h at 37 °C. For purification of Strep-tagged YqjH, cells were harvested, resuspended in 150 mM NaCl and 100 mM Tris-HCl (pH 8.0), and disrupted by using a French press (Thermo Scientific), and the filtered lysate was subjected to Strep-Tactin chromatography using an FPLC purifier system (Pharmacia) and a column with 2 mL of Strep-Tactin Superflow material (IBA). The recombinant protein was eluted with 2.5 mM D-desthiobiotin (IBA), following dialysis against the desired experimental buffer. Pure protein fractions determined by SDS−PAGE were concentrated using centrifugal filter devices with a 10000 molecular weight cutoff. Protein concentrations were determined by the Bradford method[29] using a BSA calibration curve. Protein was shock-frozen in liquid nitrogen and stored at −80 °C.

Site-Directed Mutagenesis. For introduction of single-amino acid exchanges into YqjH, the expression vector construct pMM30-3 was used as a template for site-directed mutagenesis. Overlapping primers with mutations that introduce alanine codons at desired sites were used for template amplification with Phusion HF DNA polymerase (New England Biolabs). To exchange codon 55 (K to A exchange), we used primers 5′-GACGATGATCACAGCGCACTCTTCTTTCCTCAACCTGACGCTCAC-3′ and 5′-GTTGAGGAAAGAAGAGTGCGCTGTGATCGTCAAAGCCACGCG-3′. To change codon 130 (R to A exchange), we used primers 5′-CTTACGGTGGCAGGTCCGGCCGGTTCGCTGGTGGTGCCG-3′ and 5′-CGGCACCACCAGCGAACCGGCCGGACCTGCCACCGTAAG-3′. To change codon 246 (R to A exchange), we used primers 5′-TATGACCCACAGCGGGTAGCTGCAGCGGCTTACTGGCAC-3′ and 5′-GTGCCAGTAAGCCGCTGCAGCTACCCGCTGTGGGTCATA-3′ (changed codons underlined). Remaining methylated template DNA from the dam^+ parent strain was digested with *Dpn*I (New England Biolabs), and the plasmid DNA from these reactions was subsequently transformed into *E. coli* TOP 10. Isolated plasmids were sequenced to confirm the presence of site-directed mutations. The alanine-substituted protein variants were then produced in *E. coli* BL21 as described above.

Synthesis of Aryl-Capped Oligopeptides by Solid Phase Peptide Synthesis. The unprotected compound 2,3-dihydroxybenzoic acid (DHB) was purchased from Sigma-Aldrich, and protected amino acids Fmoc-Gly-OH, Fmoc-Thr(tBu)-OH and Fmoc-Ser(tBu)-OH were purchased from Novabiochem. Oligopeptides DHB-Gly-Thr and DHB-Ser were synthesized following a standard Fmoc-based solid phase peptide synthesis protocol by using an Apex 396 peptide synthesizer (AAPPTec). Briefly, 0.1 g of 2-chlorotrityl chloride resin was washed with 5 mL of DCM; 0.2 mmol of Fmoc-protected amino acids (0.5 M DMF solution) and 0.8 mmol of DIPEA (2 M DCM solution) were added to the resin. The reaction mixture was incubated at room temperature (400 rpm for 2 h) and washed three times with DMF. After the sample had bound to the resin, the Fmoc protecting group of the primary amino function was removed by incubation in 5 mL of a 20% DMF solution of piperidine at room temperature (400 rpm for 20 min). The peptidyl-resin was washed three times with DMF. To couple the next building block, 0.3 mmol of Fmoc-protected amino acid or DHB (0.5 M DMF solution), 0.3 mmol of HBTU (0.5 M DMF solution), 0.3 mmol of HOBT·H_2O (1 M DMF solution), and 1 mmol of DIPEA (2 M DCM solution) were added to the peptidyl-resin. After incubation at room temperature (400 rpm for 1 h), the peptidyl-resin was washed three times with DMF. The peptides were cleaved from the resin by incubation in 3 mL of DCM containing 10% acetic acid and 20% trifluoroethanol at room temperature (400 rpm for 1 h); 150 mL of *n*-hexane was added to the supernatant. Removal of solvent under vacuum followed by two additional washes with *n*-hexane yielded a white solid. Subsequent treatment with trifluoroacetic acid (TFA), triisopropylsilane (TIPS), and water in a ratio of 95:2.5:2.5 (v/v) yielded the deprotected linear peptide acids. The peptides were precipitated in ice-cold diethyl ether, dissolved in DMSO, and purified by semipreparative HPLC (Agilent 1100 system) with a reversed phase 250/21 Nucleodur 100-5 C18ec column (Macherey and Nagel). The purity of the eluted oligopeptides was analyzed by ESI-Q-TOF-MS.

Preparation of Ferric Ligands. The different siderophores were obtained by chemical synthesis as in the case

of the aryl-capped peptides (described above), enterobactin[30] and MECAM.[31−33] Vibriobactin and hydroxamate siderophores were obtained from EMC Microcollections (Tübingen, Germany), and citrate was purchased from Sigma-Aldrich. The apo siderophores were charged with ferric iron by using a freshly prepared $FeCl_3$ stock solution in a 1:1 iron:ligand molar ratio in the case of intact triscatecholate and hydroxamate scaffolds, a 1:2 molar ratio in the case of citrate, and a 1:3 molar ratio in the case of the aryl peptides. All ferric ligands were prepared in Tris-buffered solution at pH 8.0 or, in some cases, pH 8.5.

UV−Vis Spectroscopy. For measurments of spectra of the oxidized enzyme, purified protein was diluted to the desired concentration in 100 mM Tris-HCl (pH 8.0) and 150 mM NaCl, and the solution was placed in a quartz cuvette (n = 1 cm). Spectra of the reduced protein were recorded under anaerobic conditions (95% N_2/5% H_2). The anaerobic solution of enzyme and substrates was placed into a tightly sealed cuvette, and spectra were recorded using an Ultrospec 3000 spectrophotometer. Data sets were analyzed with SWIFT Scan version 2.06. For the determination of the extinction coefficient of bound FAD according to common protocols,[34] the flavoprotein solution was treated (after recording the UV−vis spectrum) with 2 M urea (final concentration) to initiate unfolding of the protein, and then with 5% (w/v) TCA (final concentration) for complete protein precipitation. After a short incubation at 4 °C for 5 min, the white precipitate was removed by centrifugation, and the yellow supernatant was titrated back to pH 8.0 with a 2 M Tris solution. The free FAD was then quantified by using the extinction coefficient of 11300 M^{-1} cm^{-1} for 450 nm. For the determination of further extinction coefficients, including those of reduced FAD species, the FAD quantitation factor of the initially used oxidized form was used as a base.

UV−Vis Redox Titration. An anaerobic solution of holo-YqjH (final concentration of 36 μM) in 50 mM Tris-HCl (pH 8.0) was titrated with dithionite or NADPH in the presence of 10 μM methyl viologen, benzyl viologen, and anthraquinone 2-sulfonate as redox mediators by using a Pt(Ag/AgCl) electrode with a digital multimeter (Conrad Electronic) while the sample was mixed constantly. After redox equilibration at each titration step, aliquots were taken, and the protein fraction was separated anaerobically by fast gel filtration using Econo-Pac 10DG columns (Bio-Rad) and then analyzed by UV−vis spectroscopy. After normalization, including volume correction, logarithmic ratios of oxidized and reduced species were plotted against observed redox potentials E [vs the normal hydrogen electrode (NHE)], and midpoint potentials of the corresponding redox pairs were determined by standard regression analysis.

Fluorescence Titration. A purified recombinant protein solution in 150 mM NaCl and 100 mM Tris-HCl (pH 8.0) was adjusted to the desired concentration, and 2 mL was added to a 1 cm × 1 cm quartz cuvette. The cuvette was placed into an FP-6500 spectrofluorimeter (Jasco) and thermostated at 20 °C. Concentrated ferric siderophore stock solutions were freshly prepared and added stepwise to the protein solution. Tyrosine/tryptophan fluorescence emission at 340 nm (slit width 5 nm) was measured upon excitation at 280 nm (slit width 5 nm). Fluorescence data were normalized to a 100% starting intensity and fitted by nonlinear regression analysis (KaleidaGraph version 3.52) using the following equation according to the law of mass action:

$$F = ([P]_t - [L]_t - K_D)\frac{f_P}{2} + ([L]_t - [P]_t - K_D)\frac{f_L}{2} + ([P]_t + [L]_t + K_D)\frac{f_{PL}}{2} + (f_P + f_L - f_{PL}) \times \sqrt{\frac{([P]_t + [L]_t + K_D)^2}{4} - [P]_t[L]_t}$$

where $[P]_t$ and $[L]_t$ represent the total protein and ligand concentrations, respectively, at each titration step, f_P, f_L, and f_{PL} are the relative molar fluorescence coefficients of the free protein, the free ligand, and the protein−ligand complex, respectively, and K_D is the dissociation constant.

Enzyme Kinetics. All kinetic studies were performed under an anaerobic atmosphere (5% H_2 in N_2) in anaerobic solutions of 50 mM Tris-HCl (pH 8.0) and 100 mM NaCl at 25 °C. At first, time-dependent kinetics were assessed to determine the linear range of substrate conversion. Then, ferric substrate-dependent kinetics were assessed in the presence of excess NADPH (final concentration of 2 mM) with 2 μM holo-YqjH (native enzyme or mutagenized derivatives) in 200 μL assay volumes. Reaction mixtures were analyzed by addition of 0.15% (w/v) Ferene to detect the formation of Fe(II) by the readily formed Fe(II)−Ferene complex at an absorbance of 590 nm. Absolute quantification of generated Fe(II) was conducted by using a defined Fe(II)−Ferene calibration curve recorded at the same wavelength. Substrate concentrations were plotted against the observed rates of conversion expressed as specific activities, and kinetic parameters were calculated upon fitting according to the Michaelis−Menten model. Quantification of Fe(II) generated per NADPH equivalent was conducted in reaction mixtures containing 2 μM YqjH, 50 μM ferric siderophore, and varied concentrations of NADPH. Each point was taken at equilibrium after incubation for 30 min. To analyze the reaction mechanism, varied concentrations of ferric (2,3-dihydroxybenzoylserine)$_3$ (5−100 μM) were set together with fixed concentrations of NADPH (10, 20, 50, and 200 μM) under the aforementioned conditions. Steady state reaction rates were determined accordingly, and double-reciprocal plots were used to dissect the possible reaction types from the obtained curve slopes.

Analytical Gel Filtration. Under anaerobic conditions (95% N_2 and 5% H_2) at 25 °C, a Zorbax GF-250 column was equilibrated with anaerobically equilibrated buffer containing 150 mM NaCl and 100 mM Tris-HCl (pH 8.0) using an Agilent HPLC system (1200 series). The column was calibrated using a mixture of ferritin (440 kDa), aldolase (158 kDa), conalbumin (75 kDa), ovalbumin (44 kDa), carbonic anhydrase (29 kDa), and aprotinin (6.5 kDa) at a flow rate of 0.5 mL/min. Then, 100 μg of purified YqjH was applied at the same flow rate and temperature. UV spectra at 280 nm were recored and analyzed with Agilent ChemStation version B.03. Further, 10 μg (0.5 μM in solution) of YqjH was incubated either without or with 10 mM dithionite or 1 mM NADPH for 10 min prior to application to the column to determine possible reduction-dependent oligomerization or any detrimental effects of the high reductant concentrations on the global folding status.

Cofactor Reconstitution. To replace the native FAD cofactor by a redox-inert analogue, protein denaturing and refolding using 5-deaza-5-decarba-FAD (kindly provided from a stock of S. Ghisla, University of Konstanz, Konstanz, Germany)

was performed. Briefly, purified YqjH was diluted to 5 μM in 6 M guanidinium chloride, 150 mM Tris-HCl (pH 9.0), 1 mM EDTA, 10 mM β-mercaptoethanol, and 10 mM dithiothreitol. Aliqouts of 0.5 mL of this solution were passed through DG10 desalting columns (Bio-Rad) equilibrated with 50 mM Tris-HCl (pH 7.5) and 1 mM dithiothreitol for removal of the FAD cofactor and to initiate protein refolding. The eluted colorless apoprotein was concentrated using centrifugal filter units with a 10000 molecular weight cutoff (Millipore). The apoprotein was then diluted to 20 μM in 50 mM Tris-HCl (pH 7.5) containing 95 μM 5-deaza-5-carba-FAD. After incubation for 12 h at 15 °C, the solution was diluted 20-fold with 50 mM Tris-HCl (pH 7.5) and concentrated again. After three washing and concentration steps, reconstituted protein (75 μM) was obtained for experimental analysis.

EPR Analysis. Purified YqjH (100 μM) was reduced anaerobically with dithionite for 5 min. The EPR spectrum of the FAD semiquinone radical was measured at 80 K with a 9.4679 GHz microwave frequency, a 0.02 mW microwave power, a 100 kHz modulation frequency, and a 1.05 mT modulation amplitude using a Bruker EPR spectrometer. Further, EPR spectra of 30 μM Fe-Ent in 50 mM Tris-HCl (pH 7.5) in the absence or presence of 75 μM YqjH-WT or 75 μM YqjH reconstituted with 5-deaza-FAD were recorded at 77 K with a 9.433 GHz microwave frequency, a 20 mW microwave power, a 100 kHz modulation frequency, and a 1.25 mT modulation amplitude.

EPR Redox Titration. Fe-Ent (30 μM) together with 2.5-fold molar excess of 5-deaza-FAD-reconstituted YqjH in 50 mM Tris-HCl (pH 8.5) was anaerobically incubated and mixed with redox mediators methyl viologen, benzyl viologen, neutral red, safranine T, phenosafranine, and anthraquinone 2-sulfonate (10 μM each). Actual redox potentials were determined continuously by using a platinum electrode and a Ag/AgCl reference electrode while the protein/indicator solution was constantly mixed. Increasing amounts of dithionite were added stepwise until the lower redox plateau obtained under these conditions was reached at approximately −565 mV/NHE. Immediately frozen samples were measured at 77 K with a 9.425 GHz microwave frequency, a 20 mW microwave power, a 100 kHz modulation frequency, and a 1.25 mT modulation amplitude. For spin quantifications, a 1 mM Cu(II)-EDTA standard was used under identical conditions. Spectra were analyzed with WIN-EPR version 2.11 (Bruker Analytik GmbH), and the amplitude changes of the g = 6.60 feature were taken as a measure for the proportions of YqjH-bound ferric versus ferrous iron−ligand species. Logarithmic ratios of oxidized and reduced species were plotted against E (vs NHE) to determine the midpoint redox potential of the YqjH−ferric enterobactin complex.

Analytical HPLC−MS Analysis. For a complete desalting of proteins by HPLC using an Agilent 1100 system, samples were applied to a monolithic 50/1 ProSwift RP-4H column (Dionex). Desalted proteins were eluted by the following gradient of A (water/0.05% formic acid) and B (acetonitrile/0.045% formic acid) at a column temperature of 40 °C and flow rate of 0.2 mL/min: isocratic elution with 5% A for 2 min followed by a linear gradient to 95% B within 8 min and holding 95% B for an additional 4 min. For cofactor detection, the holoprotein was denatured by addition of 95% methanol (final concentration). Precipitated protein was removed by centrifugation, the supernatant dried under vacuum, and the remaining pellet dissolved in water. Negative ions within the mass range of m/z 500−2000 in this sample were then detected by HPLC-coupled FTICR-MS using a Finnigan LTQ-FT instrument.

CD Measurements. CD measurements of native YqjH as well as exchange derivatives K55A and R130A were conducted at 20 °C using a J-810 spectropolarimeter (JASCO). For spectral analysis in the far-UV region (190−250 nm), 4 μM protein in 1 mM Tris-HCl (pH 8.5) was measured in a 0.1 cm path length cuvette. In the near-UV−vis region (300−550 nm), 45 μM protein in 5 mM Tris-HCl (pH 8.5) was measured in a 0.5 cm path length cuvette. Spectra were recorded with a bandwidth of 1 nm, a data pitch of 0.5 nm, a response of 1 s, and standard sensitivity. The scanning speed was 100 nm/min, and data were accumulated from five scans each. All curves were corrected for the corresponding buffer signal.

Mutant Construction and Growth Analysis. *E. coli* single-deletion mutants of genes *entC*, *yqjH*, and *fes* in strain background BW25113 were obtained from the Keio Collection (Keio University, Tokyo, Japan).[35] For combination of deleted loci, ∼300 bp upstream and downstream of the *yqjH* and *fes* genes were amplified and fused with appropriate resistance cassettes by PCR.[36] The hybrid constructs were used for transformation into the kanamycin resistant *E. coli* Δ*entC* strain carrying λ Red expression plasmid pKD46.[37] Chromosomal DNA of selected mutant strains was isolated, and deletions were confirmed by PCR. For growth analysis, strains were grown in LB medium until an OD_{600} of 1.0 was reached and then diluted to an OD_{600} of 0.001 in M63 minimal medium[38] (pH 7.0) containing 0.5% (w/v) glucose as carbon source, which was further supplemented with different iron-charged siderophore ligands or $FeCl_3$ to a final concentration of 20 μM each. Cells were incubated at 37 °C and 200 rpm for 16 h, before optical densities of stationary cultures were determined spectrophotometrically. Average growth values from three independent replicates were plotted together with their corresponding standard deviations.

RESULTS

YqjH Belongs to a ViuB Homologue Subgroup with Varied Structural Features. On the basis of the ViuB founding sequence of the SIP family, homologues of this protein are found to be widely distributed in bacteria, most frequently among Proteobacteria, but also in other phyla such as Planctomycetes or Actinobacteria. However, comparative sequence analysis reveals that a homologue subgroup exists within the different classes of Proteobacteria that displays distinct variations in global protein architecture (Figure 1A). Indeed, two different subfamilies of SIPs can be distinguished on the basis of N-terminal and C-terminal sequence alterations. The first and more widespread group ("group I") contains a prominent C-terminal α-helical element. The secondary structure composition and conservation of residues are further varied within this group, leading to further differentiation from the ViuB template as observed among several members of the Actinobacteria. In contrast to group I, the C-terminal α-helix is missing in SIP homologues from a more closely related group, which includes members from the Enterobacteriales or Pseudomonadales ("group II"). The homologues from the second group possess, on the other hand, sequence extensions and insertions in the N-terminus that, however, are predicted to exhibit primarily random-coil conformation without significant proportions of α-helical or β-sheet motifs.[39,40] Inspection of the crystal structure of the ViuB homologue from *S. putrefaciens*,

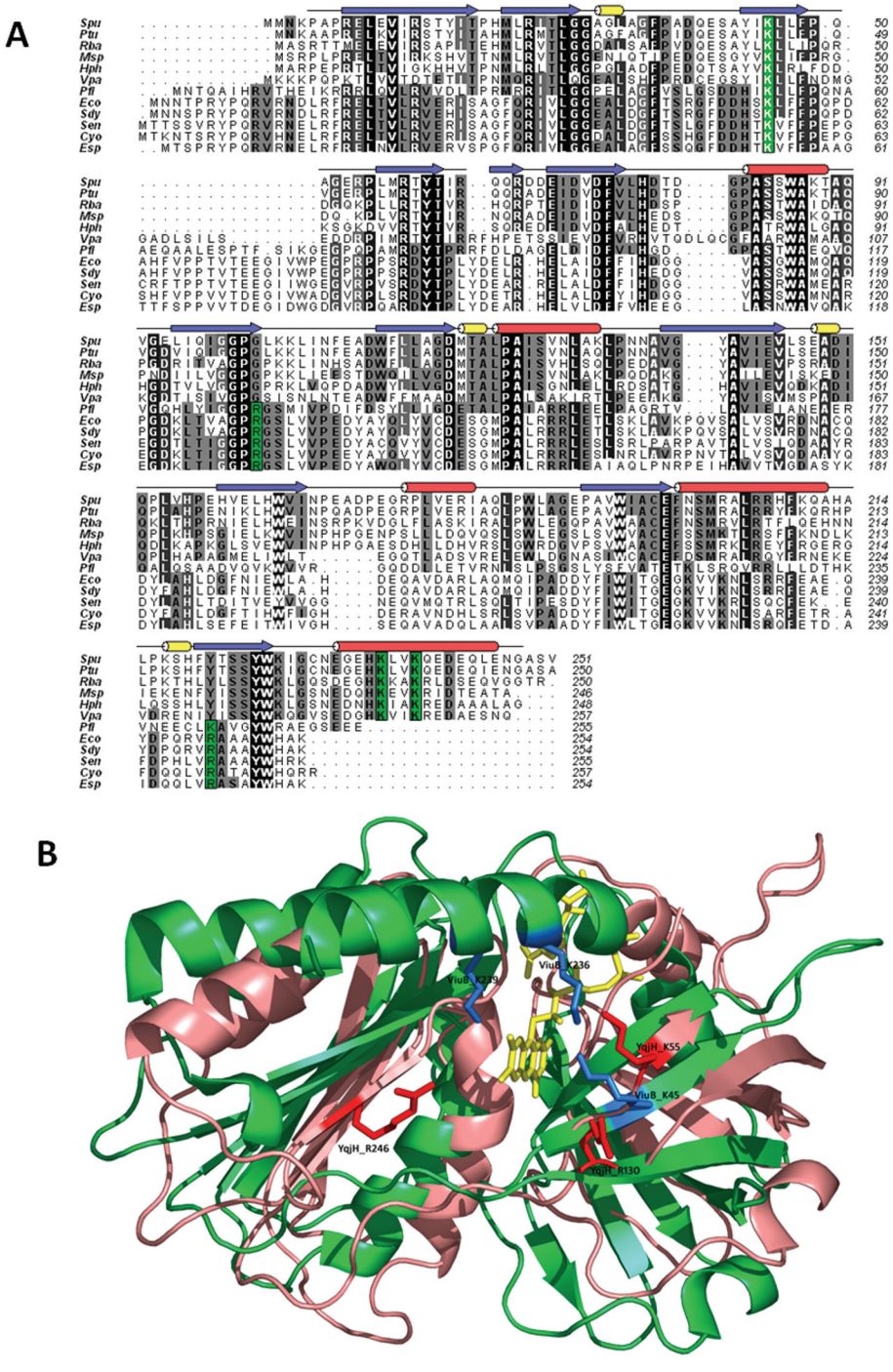

Figure 1. (A) Multiple-protein sequence alignment of ViuB-type homologues from Gram-negative representatives that reveals two different ViuB subgroups with differences in the N- and C-terminal regions. Secondary structural elements according to the ViuB homologue structure from *S. putrefaciens* are denoted by blue arrows (β-sheet elements) as well as yellow and red columns (shorter and longer α-helical elements, respectively). Conserved basic residues associated with the potential substrate binding regions of group I or group II ViuB homologues are highlighted in green. Abbreviations: Spu, *S. putrefaciens*; Ptu, *Pseudoalteromonas tunicata*; Rba, *Rhodopirellula baltica*; Msp, *Marinomonas* sp. MWYL1; Hph, *Hoeflea phototrophica*; Vpa, *Vibrio parahemolyticus*; Pfl, *Pseudomonas fluorescens*; Eco, *E. coli* K12; Sdy, *Shigella dysenteriae*; Sen, *Sa. enterica*; Cyo, *Citrobacter youngae*; Esp, *Enterobacter* sp. 638. (B) Structural model of *E. coli* YqjH (colored salmon red) generated by ESyPred3D based on the structural template of the ViuB homologue from *S. putrefaciens* (colored green together with the FAD cofactor colored yellow, PDB entry 2GPJ). Conserved basic residues spatially close to the potential substrate binding pocket are colored red in the *E. coli* YqjH model and blue in the *S. putrefaciens* ViuB homologue structure. According to the primary sequence alignment, the C-terminal α-helical element is missing in YqjH.

which belongs to the first group, showed that the C-terminal α-helix is part of a motif that in the tertiary structure forms a potential substrate binding pocket in the proximity of the potentially electron-conferring isoalloxazine ring of the bound FAD cofactor (Figure 1B). The sequence alignment shows that the three basic residues K45, K236, and K239, which cluster around this pocket, are conserved within the group I members, and that two of these residues are part of the C-terminal α-helix. Because crystallographic data reported for *E. coli* YqjH,[24] which according to the primary sequence analysis belongs to

dx.doi.org/10.1021/bi201517h | *Biochemistry* 2011, 50, 10951–10964

the second SIP group, are still preliminary and do not provide sufficient information about the C-terminal region, a structural model was generated by in silico folding using the ESyPred3D server platform,[41] and the *S. putrefaciens* ViuB homologue as a structural template providing ~30% identity and ~50% similarity. The superimposition of the resulting YqjH structural model with the *S. putrefaciens* ViuB structure shows a similar arrangement of most predicted secondary structure elements (Figure 1B). The sequence extensions and insertions in the N-terminal region of YqjH (residues 1−14 and 65−83) were not included in the folding model because of a lack of template information for these additional sequences. Because of the missing large α-helix in the C-terminus of YqjH, the potential binding pocket appears more open and not as distinct as in the original template. A further processing of the original YqjH folding model was conducted by minimizing the rmsd values between the aligned residues of YqjH and ViuB. This resulted in a high degree of structural similarity between both folding units, except for the distinct architectures of the C-terminal regions (Figure S1A of the Supporting Information). However, also three basic residues can be found in YqjH that are distributed around this putative binding region. In contrast to those residues from members of group I, two of them are associated with the parallel and antiparallel β-sheets flanking the FAD isoalloxazine ring plane on both sides, while the third residue is located in a predicted flexible loop region. Interestingly, these three residues, K55, R130, and R246 (based on the numbering of the YqjH primary sequence), are also conserved within the primary sequences of group II, especially within those from the Enterobacteriales. Basic triad amino acid motifs have been described in many ferric siderophore binding proteins from microbial as well as mammalian sources, being directly involved in the interaction with the ferric ligands.[42−44] Hence, a closer inspection of the putative substrate binding region in YqjH was attempted.

The Redox States of YqjH Suggest the Catalysis of Stepwise Single-Electron Transfer. Prior to analysis of ferric substrate binding, the redox features of the YqjH flavoprotein were investigated. First, UV−vis spectroscopy of the aerobically purified protein confirmed the presence of an oxidized FAD cofactor (FAD_{ox}) in a holoprotein fraction of ~90%, for which an extinction coefficient (ε_{452}) of 10440 M^{-1} cm^{-1} was determined (Figure 2A), which is in agreement with recently published data.[24,26] The cofactor was released from the protein and did not precipitate upon treatment of YqjH with urea and TCA during FAD quantification, indicating its noncovalent attachment to the protein. Further, the cofactor could also be released by methanol treatment of YqjH and was detected in the supernatant fraction by LC/FTICR-MS (Figure S1B of the Supporting Information).

To examine possible oligomerization states of YqjH in its oxidized and reduced forms, we incubated the protein anaerobically without or with sodium dithionite or NADPH prior to analytical gel filtration. In comparison with an analytical standard, the main fraction (94% of the integrated UV signal) of the oxidized form eluted at a calculated size of ~28 kDa, indicating primarily monomeric status under these conditions (Figure S2 of the Supporting Information). Further gel filtrations together with the reduced forms did not yield significant differences in the retention profiles, which suggests that YqjH persists as a monomer during its different stages of oxidation and in presence of its donor substrate, NADPH.

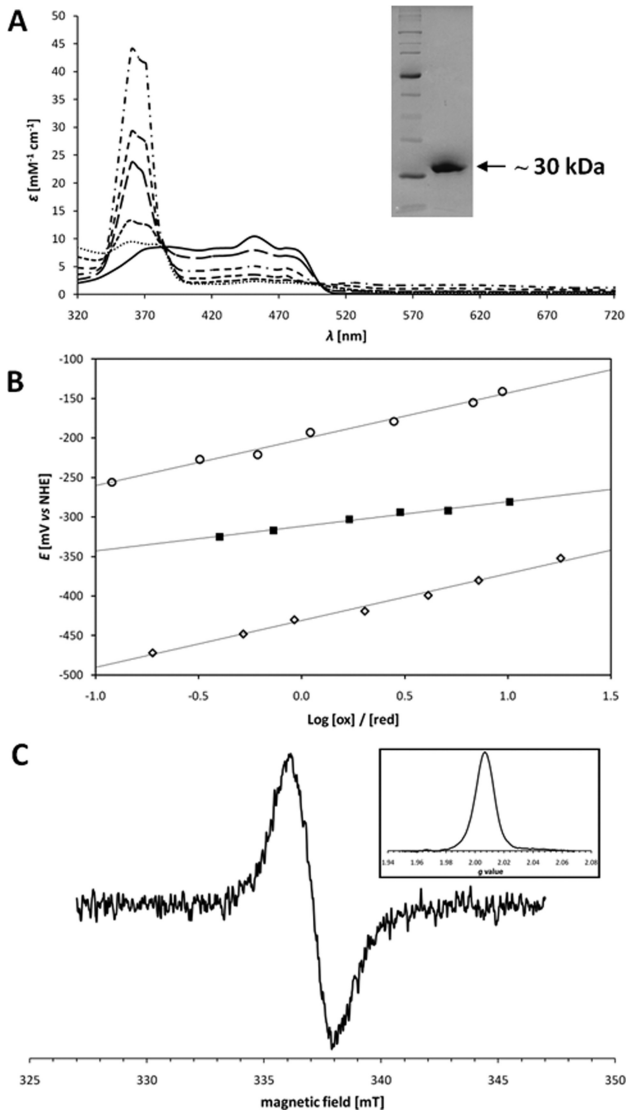

Figure 2. (A) Representative spectra from stepwise reduction of YqjH during anaerobic UV−vis redox titration with dithionite. Shown are the oxidized species at −150 mV/NHE (—), intermediate development and decrease of the semiquinone species (dashed lines), and the fully reduced hydroquinone species obtained below −500 mV/NHE (···). The inset shows SDS−PAGE results for the purified YqjH protein. (B) Plots of the redox pair ratios observed upon one-electron reduction [with dithionite; (○) FAD_{ox}/FAD_{sq} and (◇) FAD_{sq}/FAD_{hq}] or two-electron reduction [with NADPH (■)]. Logarithmic ratios vs observed redox potentials were plotted to determine electron transfer rates and midpoint potentials from linear curve slopes and x = 0 intercepts, respectively. Curve slopes were determined with 58.7 mV (FAD_{ox}/FAD_{sq}) and 59.3 mV (FAD_{sq}/FAD_{hq}) according to one-electron transfer steps and 31.1 mV (FAD_{ox}/FAD_{hq}) according to two-electron transfer steps. (C) EPR spectrum of the YqjH-bound FAD semiquinone radical measured at 80 K with a 9.4679 GHz microwave frequency, a 0.02 mW microwave power, a 100 kHz modulation frequency, and a 1.05 mT modulation amplitude. The inset shows the integration spectrum with an isotropic g factor of 2.0067.

Because a putative transfer of electrons from NADPH via the intrinsic FAD cofactor onto ferric chelate substrates suggests a switch from double- to single-electron transfer events, anaerobic redox titrations were conducted with dithionite and NADPH to examine the reduced FAD species (Figure 2). After equilibration and removal of the reductant by rapid size

exclusion chromatography, the UV−vis spectra of the protein fractions showed in the case of titration with dithionite the transient development of a flavosemiquinone (FAD_{sq}; ε_{452} = 5056 M^{-1} cm^{-1}, and ε_{360} = 43889 M^{-1} cm^{-1}) that finally resulted in the development of a fully reduced flavohydroquinone (FAD_{hq}; ε_{452} = 2361 M^{-1} cm^{-1}) (Figure 2A). Semiquinone development was characterized by high absorbance between 360 and 380 nm, while absorbance between 500 and 700 nm was rather low, which points to the presence of an anionic radical species. The isosbestic points of the spectra were at 385 and 501 nm, as well as at 343 nm, but only for the reduced species. Because the semiquinone turned out to be stable in the protein when anaerobically titrated, the redox potentials of the two redox couples, FAD_{ox}/FAD_{sq} (E_2) and FAD_{sq}/FAD_{hq} (E_1), were determined by using a platinum electrode, which showed fast equilibration with this protein and the redox mediators used. The plots of the logarithmic ratios of observed FAD_{ox}/FAD_{sq} species during reduction with the first electron equivalent versus their corresponding redox potentials (E) as well as those of the FAD_{sq}/FAD_{hq} ratios during the second electron reduction yielded linear curves with slopes of 59 ± 1 mV (Figure 2B). The resulting midpoint potentials (at pH 8.0) were as follows: E_1 = −431 ± 16 mV, and E_2 = −202 ± 9 mV. During a further redox titration with NADPH, the curve slope of the log(ox/red) ratios versus redox potentials was found to be 29.5 ± 2 mV, indicating the estimated two-step-only electron transfer, and gave a midpoint potential (E_m) for the FAD_{ox}/FAD_{hq} couple of −312 ± 7 mV (Figure 2B).

The stabilized FAD radical was further detected by EPR (Figure 2C). An intense signal of the semiquinone radical was observed at 80 K with an isotropic g factor of 2.0067, which is within the range of those g values reported for protein-associated flavosemiquinone species.[45] Thus, the redox features of FAD-binding YqjH point to the catalysis of transfer of single electrons from the hydroquinone, generated by the transfer of two electrons from NADPH, onto single-electron-accepting substrates. The formation of a stable semiquinone during this process suggested that single-electron transfers may not proceed in rapid succession onto a single substrate molecule bound but could rather require intermediate product release and binding of further substrate molecules until completion of the reaction cycle.

Basic Triad Residues of the YqjH Binding Pocket Permit High-Affinity Binding of Triscatecholate Substrates and Are Essential for Catalysis. To examine the effect of the basic residues located around the potential substrate binding pocket, we conducted site-directed mutagenesis to generate alanine-substituted derivatives. The produced protein variants were analyzed by CD spectroscopy to verify their folding properties (Figure S3 of the Supporting Information). Variants K55A and R130A exhibited similar spectra of secondary structure elements and of the bound FAD in the far- and near-UV regions compared with native YqjH, respectively, and hence were considered to be properly folded. In contrast, variant R246A was found to be rather unstable, showing precipitate formation and cofactor release during protein concentration, and thus was not used for further comparative studies.

Together with native YqjH and the two stable alanine-substituted variants, binding studies were then performed with different ferric siderophore ligands by using fluorescence titration analysis (Figure 3). The oxidized, noncatalytic YqjH species exhibited significantly different binding affinities toward the assayed ferric siderophore ligands. Native YqjH displayed the highest binding affinities for the ferric enterobactin ligand and its close synthetic homologue, ferric MECAM, showing dissociation constants for both in the submicromolar range. The two alanine derivatives showed comparatively weak affinities for these ligands, with estimated dissociation constants that were not in the submicromolar range. Similar differences were observed with further ferric triscatecholate ligands, including ferric vibriobactin and ferric bacillibactin as well as the hydrolyzed ferric Fe(III)−$(DHB\text{-}serine)_3$ and Fe(III)−$(DHB\text{-}glycine\ threonine)_3$ complexes (see also Figure S4 of the Supporting Information), which were obtained upon solid phase peptide synthesis of the aryl-capped short peptides and, after deprotection and HPLC purification, by iron charging in a 1:3 molar stoichiometry. Native YqjH bound these ligands with dissociation constants in the low micromolar range, while no affinity in this range was observed with the binding site variants. Ferric dicitrate was also bound by wild-type YqjH, but with an affinity at least 10-fold lower than the affinities of most of the catecholate-containing ligands. Interestingly, no significant affinity of YqjH was observed for the hydroxamate siderophores ferric aerobactin and ferrichrome, indicating either very weak or no binding of representatives from this siderophore class.

Several of the tested ligands were subsequently used as potential substrates for YqjH-catalyzed reduction in kinetic studies that were performed anaerobically. While the time-dependent reduction of ferric substrates with prominent charge-transfer absorption bands like ferric enterobactin could be followed directly by the decrease in absorption (Figure 4A), substrate-dependent kinetics in the lower concentration range were preferably performed by using sensitive detection of a Fe(II)−ferene complex at 590 nm, a wavelength that further did not interfere with cofactor absorbance. The kinetic data were fitted because of their Michaelis−Menten-like behavior for both native and substituted YqjH variants. According to the ligand binding studies, the substituted basic residues were found to be crucial for catalysis, because the alanine variants exhibited much lower overall catalytic efficiencies than the native enzyme (Figure 4B, Figure S5 of the Supporting Information, and Table 1). In all cases, the loss of efficiency was associated with a strong increase in K_M, suggesting the impaired ferric substrate binding due to the derivatized active site.

YqjH Shows the Highest Catalytic Efficiency for Hydrolyzed Ferric Triscatecholates and Reduces Ferric Substrates in a Double-Displacement Reaction Mechanism. In a comparison of the catalytic efficiencies obtained for native YqjH (Table 1), they were found to be highest in cases of the hydrolyzed triscatecholate substrates Fe(III)−$(DHB\text{-}serine)_3$ and Fe(III)−$(DHB\text{-}glycine\text{-}threonine)_3$. Surprisingly, though the k_{cat} is much lower, the catalytic efficiency of ferric enterobactin reduction is in the range of that of the hydrolyzed ferric bacillibactin Fe(III)−$(DHB\text{-}glycine\ threonine)_3$ complex that, however, is still more than 2 times less efficiently converted than the Fe(III)−$(DHB\text{-}serine)_3$ complex. The remarkable efficiency of intact ferric enterobactin can primarily be explained by its very low K_M of 0.4 μM, which is in good agreement with the observed dissociation constant that relates the velocity constants of substrate dissociation (k_{-1}) and association (k_1). In contrast to enterobactin, ferric vibriobactin conversion was less efficient, although its acceptance as a substrate indicates that YqjH releases iron not only from triscatecholate−trilactone scaffolds but also from nonhydrolyzable triscatecholates, however with lower efficiency. Also the

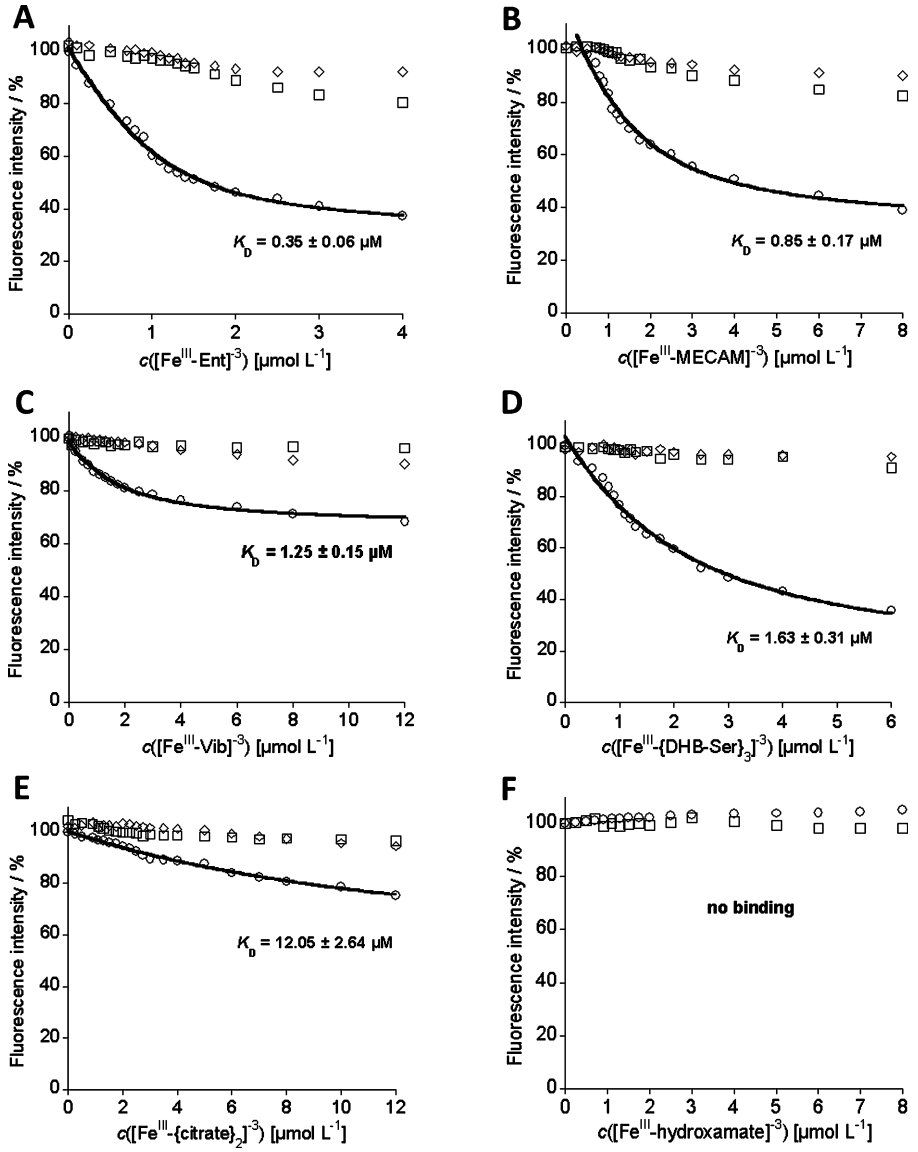

Figure 3. Determination of ligand binding affinities by fluorescence titration with native YqjH and variants YqjH_K55A and YqjH_R130A generated by site-directed mutagenesis. (A–D) Protein variants YqjH (○), YqjH_K55A (□), and YqjH_R130A (◇), each at 1.0 μM, were titrated with ferric enterobactin (Fe-Ent), ferric MECAM (Fe-MECAM), ferric vibriobactin (Fe-Vib), and the ferric (2,3-dihydroxybenzoylserine)$_3$ complex (Fe-[DHB-Ser]$_3$), respectively. (E) Proteins YqjH (○), YqjH_K55A (□), and YqjH_R130A (◇), each at 2.5 μM, were titrated with ferric dicitrate (Fe-[citrate]$_2$). (F) YqjH at 2.5 μM was titrated with ferric hydroxamate siderophores ferrichrome (○) and ferric aerobactin (□). In cases of observed fluorescence quenching, a law of mass fit (see Materials and Methods for the equation) was used (1:1 binding stoichiometries of the protein and the indicated iron–ligand complexes gave the best fitting results according to the molar fluorescence coefficients of the protein–ligand complexes, f_{PL}). The determined dissociation constants (K_D) are given.

efficiency of ferric dicitrate reduction was found to be lower, because the relatively high turnover rate seems not to compensate for the high K_M of this substrate. No significant conversion was found for ferric aerobactin, indicating that this siderophore is not within the substrate range of this reductase according to the observed lack of binding affinity. Altogether, YqjH proves to be a ferric siderophore reductase that primarily converts hydrolyzed ferric triscatecholate complexes but further allows utilization of intact ferric triscatecholates as well as ferric dicitrate, which are associated with different iron uptake routes.[1,3]

To determine the ratio of catalyzed electron transfers per NADPH reduction equivalent, NADPH-dependent kinetics were assessed in an excess of ferric substrate, and the formation of Fe(II) was measured as a result of single-electron transfer (Figure 4C). The numbers of equivalents of Fe(II) generated per NADPH were found to be 1.32 ± 0.11 for ferric enterobactin, 1.91 ± 0.12 for the Fe(III)–(DHB-serine)$_3$ complex, 1.88 ± 0.07 for the Fe(III)–(DHB-glycine threonine)$_3$ complex, and 1.98 ± 0.04 for the Fe–dicitrate complex. The low molar ratio of reduced product relative to reduced substrate in the case of ferric enterobactin indicates that one of the two single-electron transfer steps through the reduced FAD cofactor is extremely inefficient, which in turn may explain the low turnover rates of the intact ferric triscatecholate scaffold, despite its high affinity for the catalytic pocket.

The reaction-type mechanism of YqjH was determined by using the catalytically most efficient substrate, the Fe(III)–(DHB-serine)$_3$ complex. Ferric substrate-dependent steady state kinetics were performed with four different NADPH concentrations and analyzed by double-reciprocal plots of substrate concentrations

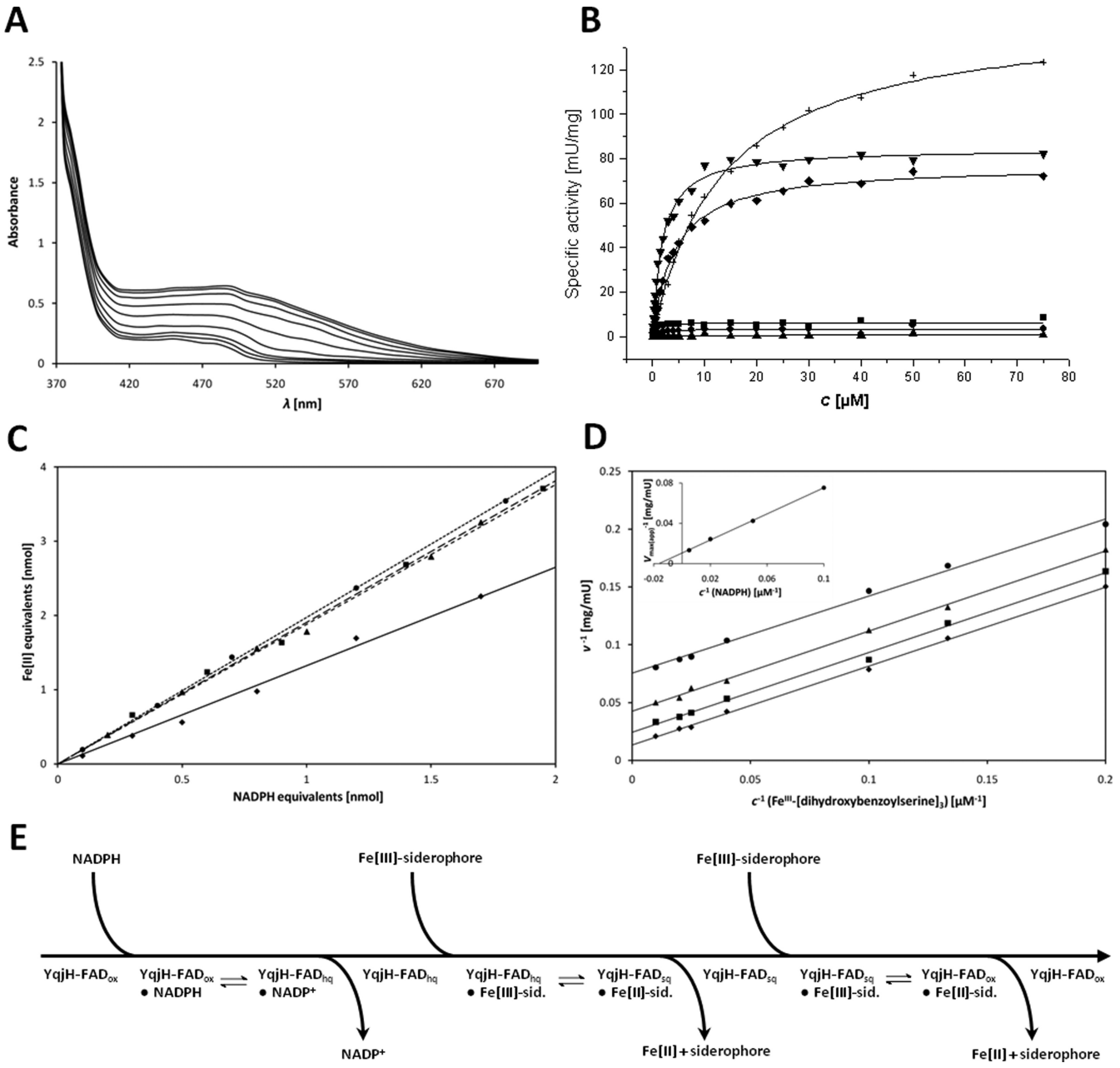

Figure 4. YqjH kinetics and reaction mechanism. (A) UV−vis spectroscopy of ferric enterobactin reduction (visible λ_{max} of charge-transfer band observed initially at 492 nm) with 75 μM Fe-Ent, 2 mM NADPH, and 20 μM YqjH in anaerobic 100 mM Tris (pH 8.0). The reaction was followed over 2.5 h with samples taken after time intervals of 0, 10, 20, 40, 60, 80, 100, 120, and 150 min. (B) Ferric substrate-dependent kinetics with 2 mM NADPH, 2 μM YqjH, and varied concentrations of ferric enterobactin (■), ferric vibriobactin (●), ferric aerobactin (▲), ferric $(DHB\text{-}serine)_3$ (▼), ferric $(DHB\text{-}Gly\text{-}Thr)_3$ (◆), and ferric dicitrate (+). (C) Equivalents of Fe(II) generated per NADPH equivalent in reaction mixtures containing 2 μM YqjH, 50 μM ferric siderophore, and varied concentrations of NADPH. Each point was taken at equilibrium after incubation for 30 min. Generated equivalents of Fe(II) per NADPH were 1.32 for ferric enterobactin (◆, solid regression line), 1.91 for ferric $(DHB\text{-}serine)_3$ (■, long dash regression line), 1.88 for ferric $(DHB\text{-}Gly\text{-}Thr)_3$ (▲, medium dash regression line), and 1.98 for ferric dicitrate (●, short dash regression line). (D) Double-reciprocal plot of steady state reaction rates with varied concentrations of ferric $(DHB\text{-}serine)_3$ (5−100 μM) and fixed concentrations of NADPH [10 (●), 20 (▲), 50 (■), and 200 μM (◆)]. The inset shows the double-reciprocal plot of the $V_{max(app)}$ y-intercept points vs NADPH concentration. The x- and y-intercepts yield apparent K_M and V_{max} values for NADPH of 62.4 μM and 96.2 milliunits/mg, respectively. (E) Proposed double-displacement (ping-pong) mechanism for the YqjH-catalyzed reaction (for substrates within the efficient redox ranges of both E_1 and E_2).

versus observed specific activities (Figure 4D). The apparent K_M and V_{max} values for NADPH were further determined by double-reciprocal plots of the $V_{max(app)}$ intercept points versus the corresponding NADPH concentrations, resulting in values of 62.4 μM and 96.2 milliunits/mg, respectively (Figure 4D). The obtained parallel curve slopes of the double-reciprocal plots strongly indicate a double-displacement reaction mechanism, which is indicated in a reaction cycle model that is exemplary for ferric substrates in the efficient redox range of E_1 and E_2 (Figure 4E). The suggested reaction cycle is initiated by the binding of NADPH, and a two-electron transfer occurs toward the oxidized flavin cofactor (FAD_{ox}). Upon dissociation of $NADP^+$, the

dx.doi.org/10.1021/bi201517h | Biochemistry 2011, 50, 10951−10964

Table 1. Kinetic Parameters of Native YqjH and Alanine-Substituted Variants

	Fe(III)−enterobactin	Fe(III)−vibriobactin	Fe(III)−aerobactin	Fe(III)−(DHB-Ser)$_3$	Fe(III)−(DHB-Gly-Thr)$_3$	Fe(III)−dicitrate
V_{max} (milliunits/mg)						
WT	6.2	3.6	1.9	84.5	77.0	145.4
K55A	0.5	nd[a]	nd[a]	7.2	nd[a]	27.8
R130A	0.9	nd[a]	nd[a]	9.6	nd[a]	16.9
K_M (μM)						
WT	0.4	1.4	48.0	1.8	4.2	13.4
K55A	7.8	nd[a]	nd[a]	40.0	nd[a]	51.0
R130A	5.9	nd[a]	nd[a]	36.0	nd[a]	66.0
k_{cat}/K_M (s^{-1} M^{-1})						
WT	8211	1268	20	23354	9193	5427
K55A	32	nd[a]	nd[a]	91	nd[a]	271
R130A	76	nd[a]	nd[a]	132	nd[a]	129

[a]Not determined.

formed hydroquinone species (FAD_{hq}) transfers a single electron to a binding ferric siderophore substrate, which is converted into the ferrous form and dissociates, while an intrinsic flavine semiquinone (FAD_{sq}) is formed, which transfers a second electron to another ferric siderophore substrate, which dissociates during regeneration of the oxidized enzyme.

High-Affinity Binding of Ferric Enterobactin Leads to a Partial Overlap with the Effective E_1 Redox Range of YqjH. In contrast to the hydrolyzed ferric triscatecholate and ferric dicitrate complexes, which display moderately low redox potentials, the capability to reduce intact triscatecholates like ferric enterobactin is still mechanistically unclear, because these ligands possess extremely negative redox potentials of approximately −750 mV.[6] Although their cytosolic potentials may partially increase because of the actual disequilibria of oxidized and reduced species, it is unknown if there is yet another mechanism that might lead to feasible reduction within the effective redox range of the enzyme. We hence attempted to determine the ferric enterobactin redox potential in the ferric substrate−YqjH complex, because it has been suggested that the redox potential of the siderophore−reductase interaction is more decisive than the potential of the free ferric siderophore when considering its actual redox capacities.[46] For this purpose, the native FAD cofactor of YqjH was replaced upon protein refolding and reconstitution with 5-deaza-5-carba-FAD, a structural analogue that is restricted to two-electron transfer steps only. Thus, by using this cofactor analogue, the native protein environment can be provided for high-affinity interaction with the ferric substrate, however, without catalytic turnover under reductive conditions. The reconstitution with 5-deaza-5-carba-FAD resulted in a protein−cofactor complex with novel UV−vis absorption features, showing several pronounced fine structures in the spectrum compared to free 5-deaza-5-carba-FAD (Figure 5A). These well-resolved vibration sidebands indicate the tight and well-defined noncovalent binding of the non-native chromophore to the ordered protein structure.

EPR spectra recorded with both native and reconstituted YqjH in presence of ferric enterobactin showed in addition to the typical high spin doublet signal (g = 4.30) a broad axial S = 5/2 signal (g = 6.60), which apparently represents a specific feature of protein-ligand interaction when compared to the free ferric enterobactin and free YqjH spectra (Figure 5B). Ferric enterobactin in the presence or absence of reconstituted YqjH was then titrated anaerobically with dithionite, and the redox potentials were measured after the equilibration of each titration step. Free ferric enterobactin did not show a significant change in the g = 4.30 signal amplitude even after addition of 25 mM dithionite to reach the lowest titration potential of approximately −565 mV/NHE (Figure S6A of the Supporting Information). In contrast, a total signal reduction of ∼30% for the complex-specific g = 6.60 signal was observed in the presence of noncatalytic YqjH (Figure S6B of the Supporting Information). The determined log(ox/red) ratios were plotted versus the corresponding equilibrium redox potentials, and a midpoint potential of the ferric enterobactin−YqjH complex could be extrapolated (E_m = −585 ± 21 mV) (Figure 5C). This large increase in the enzyme-bound substrate redox potential leads, within experimental error, to a partial overlap with the effective E_1 redox range of catalytically active YqjH. The redox potential of the ferric substrate−enzyme complex was still too low for an efficient overlap with the E_2 range that, however, may explain both the low turnover rates and the low ratio of generated Fe(II) to NADPH equivalents in the case of intact ferric enterobactin.

The Absence of YqjH Slows Growth upon Supplementation with Ferric Triscatecholates and Ferric Dicitrate. Recently, it has been reported that the combination of an *yqjH* deletion with a deletion of the *fes* esterase gene leads to an increase in the level of the severe growth phenotype, which is basically implemented by the Δ*fes* background.[26] To investigate the effect of a *yqjH* deletion on growth supplementation with different siderophores, but without intrinsic accumulation of the native siderophore enterobactin, we combined the *yqjH* and *fes* deletions in this study with an *entC* deletion background, which aborts production of both the intact triscatecholate as well as precursors such as 2,3-dihydroxybenzoylserine or 2,3-dihydroxybenzoate.[47]

The Δ*entC* single mutant, the Δ*entC* Δ*yqjH* and Δ*entC* Δ*fes* double mutants, and the Δ*entC* Δ*fes* Δ*yqjH* triple mutant were grown in iron-limited minimal medium with different ferric siderophores and with ferric chloride added to the main cultures (Figure 6). Supplementation of Δ*entC* with ferric substrates increased the rate of growth throughout, while it was impaired for the Δ*entC* Δ*fes* double deletion in the case of ferric enterobactin supplementation. In contrast, growth of the strains with the *yqjH* deletion background was more severely affected in the four cases of ferric triscatecholate and ferric dicitrate addition. Remarkably, the utilization of the nonhydrolyzable enterobactin analogue MECAM appeared to be directly dependent on the activity of YqjH. On the other hand, addition of ferric aerobactin supported all strains similarly in growth, indicating that ferric hydroxamate utilization is dependent on neither *fes* nor *yqjH*,

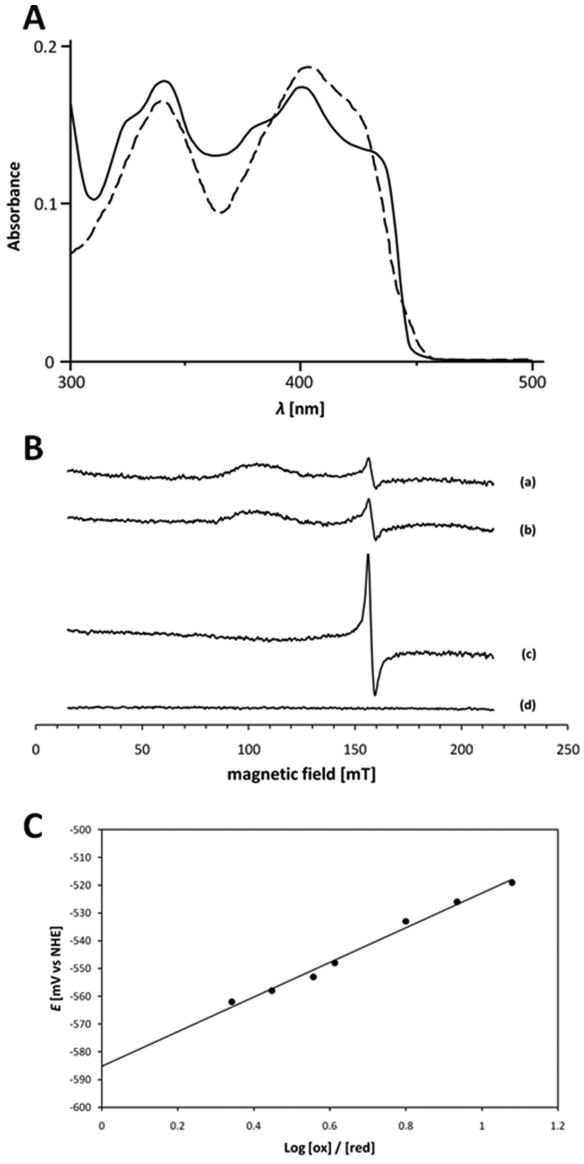

Figure 5. (A) UV−vis spectra of free 5-deaza-5-carba-FAD (−−−) and YqjH reconstituted with 5-deaza-5-carba-FAD (—). Spectra were recorded with each compound at 20 μM and pH 7.5. (B) EPR spectra of 30 μM ferric enterobactin in the presence of 75 μM WT YqjH (a), 30 μM ferric enterobactin in the presence of 75 μM YqjH-5-deaza-FAD (b), 30 μM ferric enterobactin in free form (c), and 75 μM YqjH-5-deaza-FAD (d). Spectra were recorded at pH 8.5 and 77 K with a 9.433 GHz microwave frequency, a 20 mW microwave power, a 100 kHz modulation frequency, and a 1.25 mT modulation amplitude. g values of 6.60 in spectra a and b and 4.30 in spectra a−c were observed. (C) Anaerobic single-electron redox titration of 30 μM ferric enterobactin in the presence of 75 μM noncatalytic YqjH (reconstituted with 5-deaza-5-carba-FAD) at pH 8.5. Plotted are the logarithmic ratios of protein-complexed ferric/ferrous iron−siderophore species (according to the amplitude of the binding-specific g = 6.60 signal) vs the corresponding equilibrium redox potentials. The observed curve slope was 62.3 mV according to single-electron transfer.

which is further consistent with the ligand affinity and enzyme kinetic studies for YqjH as shown above.

DISCUSSION

The presence of SIPs in many different bacterial species has raised the question of whether these proteins are directly involved in siderophore binding associated with a possible

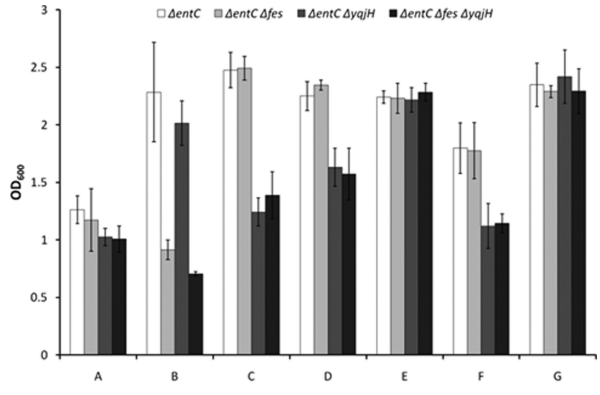

Figure 6. Mutant growth analysis with hydrolyzed or intact ferric siderophores in a chromosomal background (Δ*entC*) deficient for catecholate synthesis. *E. coli* BW25113 strains Δ*entC* (white bars), Δ*entC* Δ*fes* (light gray bars), Δ*entC* Δ*yqjH* (medium gray bars), and Δ*entC* Δ*fes* Δ*yqjH* (dark gray bars) were precultured in LB medium and then 1000-fold diluted into M63 minimal medium without an iron source in the controls (A). Further cultures were supplemented with 20 μM (final concentration) ferric enterobactin (B), ferric (2,3-dihydroxybenzoylserine)$_3$ (C), ferric dicitrate (D), ferric aerobactin (E), ferric MECAM (F), or ferric chloride (G). Final optical densities were determined after growth for 16 h, and data of three independent growth replicates were averaged and are plotted with their standard deviations.

reduction of iron. A mechanism of reductive iron assimilation upon ferric siderophore uptake is generally regarded to be crucial for the following assembly of iron−sulfur clusters and heme cofactors, for the delivery of iron into storage proteins like Dps, or for interaction with intracellular sensors such as Fur and further iron-dependent regulators.[48−51] Only recently has evidence been provided that such a reductase activity is associated with the SIP homolog YqjH from *E. coli* been provided, which was suggested to provide a link between iron and nickel homeostasis.[26] From the structural perspective, YqjH shares the domain structure of the ferredoxin reductase-like family. Ferredoxin reductase (FNR) is an FAD and NAD(P) binding protein that catalyzes the transfer of an electron from reduced ferredoxin (or sometimes flavodoxin) preferably to $NADP^+$, thereby forming $FADH_2$ via a semiquinone intermediate, which then transfers the hydride to convert $NADP^+$ to NADPH. The single-electron transfer potentials for FNR were determined to be −331 mV (FAD_{ox}/FAD_{sq}) and −314 mV (FAD_{sq}/FAD_{hq}), and a potential of −323 mV was measured for the two-electron reduction process.[52] In this study, the potential for the two-electron reduction of YqjH by NADPH was found to be similar to the FNR potential, being in the redox range of the NADPH/$NADP^+$ couple. In contrast, the redox potential gradient of the intrinsic FAD_{ox}/FAD_{sq} and FAD_{sq}/FAD_{hq} pairs is conversely arranged in YqjH, pointing to a strong preference of the flow of electrons from NADPH to ferric substrates as single-electron acceptors. While the flat redox gradient in FNR allows the reaction to be readily switched in both directions, the rather steep redox gradient for single-electron transfer in YqjH seems to restrict an uphill transfer of electrons in the direction of $NADP^+$. Thus, the general redox properties of YqjH differ from those of its structural analogue, FNR, in rather favoring the flow of electrons toward the ferric siderophore substrates, which is according to the suggestion that iron assimilation might be the primary aim of this reaction rather than NADPH generation. Mechanistically, the determined ordered ping-pong reaction type indicates that the formed

dx.doi.org/10.1021/bi201517h | *Biochemistry* 2011, 50, 10951−10964

$NADP^+$ dissociates completely before the ferric substrates are bound and reduced successively. However, sequential mechanisms may also produce ping-pong-like behavior, which is dependent on the rates of formation of a ternary complex and dissociation relative to those of electron transfer, as discussed especially for the backward reaction of FNR and further NAD(P)H:flavin oxidoreductases.[52,53] Generally, ternary species with short half-lives are hardly accessible to steady state or rapid reaction measurements. Therefore, the interpretation of the initial velocity data as a nonsequential reaction type does not necessarily exclude transitory ternary complex formation, especially in a multisite mechanistic model.[54] Interestingly, while ternary complex formation in a sequential mechanism is observed for the forward reaction of FNR leading to $NADP^+$ reduction, double-displacement reaction types seem to be more common for the reverse flow of electrons of NADPH-dependent reduction within this enzyme superfamily.[53,55,56] The YqjH reductase appears to be a further member of NADPH:flavin oxidoreductases that show double-displacement-type kinetics, without excluding a possible formation of very short-living higher-order complexes.

Protein−siderophore complex formation is accomplished in several proteins through basic amino acid residues such as lysine and arginine. These residues participate in the interaction with ferric ligands, either by mixed electrostatic/cation-π binding of the aromatic core motif in ferric triscatecholates[42] or by primarily electrostatic binding of the iron-coordinating oxo-donor motif.[43,44] The replacement of two basic residues that were predicted to constitute a part of the substrate binding site of YqjH had a strong impact on both ferric substrate interaction and conversion. High-affinity binding was abolished in the single-alanine substitution variants K55A and R130A, which led to a drastic decrease in catalytic efficiency especially in the cases of intact and hydrolyzed ferric triscatecholate substrates. In the case of ferric enterobactin, the high-affinity binding mode seems to represent a key for overlapping the substrate redox potential with the enzyme redox range. The ferric ligand displayed an increase in its midpoint potential in the enzyme−substrate complex, which could be due to partial distortion of the geometry of the iron−oxo center during the tight interaction with the basic amino acid triad. Because a further affinity increase might become counterefficient because of slow dissociation of the enzyme−product complex (the similar K_M and K_D values indicate that k_2 becomes much lower than k_{-1}), a partial overlap with the efficient E_1 redox range could be sufficient for reducing nonhydrolyzed ferric triscatecholate complexes, though at low catalytic rates. The observed low k_{cat} might be increased if ferrous iron sinks are supplied in the cytosol, as it was shown exemplarily in vitro for a ferric siderophore reductase in the presence of a metal-scavenging protein scaffold.[27] A further cause for the observed low turnover rates in vitro might be the slow disproportionation of the formed flavosemiquinone species in the E_1-dependent half-reaction. When free in solution, flavosemiquinone radicals rapidly disproportionate to their oxidized and reduced forms, but they are much less prone to dismutation when shielded by the protein environment.[52] In vivo, however, the E_2-dependent electron transfer step leading to regeneration of the oxidized form could be more readily completed by utilization of alternative ferric substrates with higher midpoint potentials, such as hydrolyzed ferric triscatecholate species or ferric dicitrate. These substrates were all found to provide nearly 2-fold molar ratios of generated Fe(II) to applied NADPH equivalents.

The capacity of YqjH to catalyze ferric enterobactin reduction by partial oxidation of its flavin cofactor leads to a rationale for the observed growth support of *E. coli* cultures in the presence of nonhydrolyzable ferric triscatecholates, which was reported in previous studies.[57−59] In this study, the supporting growth effect observed in the presence of ferric MECAM was indeed found to depend on the presence of YqjH. Effects of *yqjH* deletion were studied in combination with deletion backgrounds of both catecholate siderophore biosynthesis (Δ*entC*) and triscatecholate trilactone hydrolysis (Δ*fes*). When iron-charged catecholate and citrate siderophore substrates were supplied to the cultures with a *yqjH* deficiency, growth reduction of at least 20% was observed during the stationary phase, indicating that YqjH acts in iron acquisition pathways that utilize these siderophores as primary iron sources. In the case of ferric enterobactin, which is the highest-affinity siderophore of *E. coli*, the deletion of the *fes* esterase was decisive for the strongly impaired growth phenotype, which was further diminished when combined with the mutation of *yqjH*. This suggests that YqjH does not act in parallel, but downstream of the Fes reaction, which in a previous step produces hydrolyzed ferric triscatecholate species with much more favorable redox potentials for YqjH. The possibility of YqjH reducing ferric enterobactin in its intact form could, on the other hand, become important during intermediate stages of cytosolic overaccumulation of this siderophore, in which YqjH might act as a supporting factor for its turnover, or in situations that require strong reductive iron assimilation in combination with a high concentration of unoccupied Fe(II) binding sites. Alternatively, the genetic results may further indicate that YqjH might be involved in a parallel but less important pathway for catecholate siderophore utilization, thereby producing a synthetic phenotype when it is deleted in combination with Fes. However, it seems most consistent that YqjH may be used to reduce ferric iron associated with enterobactin cleavage products or enterobactin precursors that are secreted on their own. In the absence of Fes, the reductase could also use the overaccumulated intact ferric enterobactin as a substrate.

In contrast to YqjH, the ViuB protein from *V. cholerae* that belongs to group I of SIPs containing the C-terminal α-helical element as a part of the substrate binding pocket could complement a *fes* mutation in *E. coli*.[22] This points to the manifestation of dissimilar reductive capacities between the different structural subgroups of this enzyme family. Because *V. cholerae* produces nonhydrolyzable vibriobactin, it may require a reductase that primarily reduces iron in the intact scaffold of the triscatecholate siderophore. In contrast, Enterobacteria that commonly produce hydrolyzable enterobactin possess the Fes esterase frequently together with the YqjH type (group II) of the SIP family. Because YqjH is efficient for reduction of the hydrolyzed rather than the intact ferric triscatecholate complexes, the two dissected homologue SIP groups may illustrate different evolutionary results of reductive iron assimilation based on the preprocessing capacity for ferric triscatecholate scaffolds. Further analysis of SIP representatives, especially from group I, is needed to understand the role of this enzyme family in cytosolic iron assimilation, as well as its integration in the interwined regulation of cellular metal homeostasis.

■ ASSOCIATED CONTENT

Supporting Information

rmsd-minimized structural model of YqjH, mass detection of the FAD cofactor, gel filtration profiles of YqjH, CD spectra of native YqjH and alanine-substituted derivatives, fluorescence titrations with native YqjH and its variants, kinetics of YqjH variants, and EPR spectra of redox titrations of free ferric enterobactin and YqjH reconstituted with 5-deaza-5-carba-FAD. This material is available free of charge via the Internet at http://pubs.acs.org.

■ AUTHOR INFORMATION

Corresponding Author

*Telephone: +49 (0)6421 2825794. Fax: +49 (0)6421 2822191. E-mail: miethke@staff.uni-marburg.de.

Funding

This work was funded by the Deutsche Forschungsgemeinschaft (DFG) and the SYNMIKRO-LOEWE center (Marburg, Germany).

■ ACKNOWLEDGMENTS

We thank O. Burghaus and A. J. Pierik (University of Marburg, Marburg, Germany) for supporting EPR studies and redox titrations, S. Ghisla (University of Konstanz) for a sample of deaza-FAD, the Keio Collection for providing *E. coli* mutant strains, and J. Wertz (CGSC, Yale University, New Haven, CT) for providing plasmid pKD46. Further, we thank S. C. Andrews (University of Reading, Reading, U.K.), F. W. Outten (University of South Carolina, Columbia, SC), K. Hantke (University of Tübingen, Tübingen, Germany), and T. Giessen (University of Marburg) for helpful discussion of preliminary experimental data.

■ ABBREVIATIONS

aTc, anhydrotetracycline; BB, bacillibactin; CD, circular dichroism; DCM, dichloromethane; DHB, 2,3-dihydroxybenzoate; DIPEA, diisopropylethylamine; DMF, *N*,*N*-dimethylformamide; DMSO, dimethyl sulfoxide; EDTA, ethylenediaminotetraacetic acid; Ent, enterobactin; EPR, electron paramagnetic resonance; ESI-Q-TOF-MS, electrospray ionization quadrupole time-of-flight mass spectrometry; FAD, flavin adenine dinucleotide; Fmoc, 9-fluorenylmethoxycarbonyl; FPLC, fast performance liquid chromatography; FTICR-MS, Fourier transform ion cyclotron resonance mass spectrometry; HBTU, 2-(1*H*-benzotriazol-1-yl)-1,1,3,3-tetramethyluronium hexafluorophosphate; HPLC, high-performance liquid chromatography; hq, hydroquinone; MS, mass spectrometry; NAD(P)H, nicotinamide adenine (phosphate) dinucleotide; NHE, normal hydrogen electrode; rmsd, root-mean-square deviation; SDS−PAGE, sodium dodecyl sulfate−polyacrylamide gel electrophoresis; SIP, siderophore-interacting protein; sq, semiquinone; tBu, *tert*-butyl; TCA, trichloroacetic acid; TFA, trifluoroacetic acid; TIPS, triisopropylsilane; Tris, tris(hydroxymethyl)-aminomethane; Vib, vibriobactin.

■ REFERENCES

(1) Andrews, S. C., Robinson, A. K., and Rodriguez-Quinones, F. (2003) Bacterial iron homeostasis. *FEMS Microbiol. Rev. 27*, 215−237.

(2) Hider, R. C., and Kong, X. (2010) Chemistry and biology of siderophores. *Nat. Prod. Rep. 27*, 637−657.

(3) Miethke, M., and Marahiel, M. A. (2007) Siderophore-based iron acquisition and pathogen control. *Microbiol. Mol. Biol. Rev. 71*, 413−451.

(4) Pierre, J. L., Fontecave, M., and Crichton, R. R. (2002) Chemistry for an essential biological process: The reduction of ferric iron. *BioMetals 15*, 341−346.

(5) Harrington, J. M., and Crumbliss, A. L. (2009) The redox hypothesis in siderophore-mediated iron uptake. *BioMetals 22*, 679−689.

(6) Cooper, S. R., McArdle, J. V., and Raymond, K. N. (1978) Siderophore electrochemistry: Relation to intracellular iron release mechanism. *Proc. Natl. Acad. Sci. U.S.A. 75*, 3551−3554.

(7) Loomis, L. D., and Raymond, K. N. (1991) Solution equilibria of enterobactin and metal-enterobactin complexes. *Inorg. Chem. 30*, 906−911.

(8) O'Brien, I. G., and Gibson, F. (1970) The structure of enterochelin and related 2,3-dihydroxy-N-benzoylserine conjugates from *Escherichia coli*. *Biochim. Biophys. Acta 215*, 393−402.

(9) Hantke, K., Nicholson, G., Rabsch, W., and Winkelmann, G. (2003) Salmochelins, siderophores of *Salmonella enterica* and uropathogenic *Escherichia coli* strains, are recognized by the outer membrane receptor IroN. *Proc. Natl. Acad. Sci. U.S.A. 100*, 3677−3682.

(10) Griffiths, G. L., Sigel, S. P., Payne, S. M., and Neilands, J. B. (1984) Vibriobactin, a siderophore from *Vibrio cholerae*. *J. Biol. Chem. 259*, 383−385.

(11) Cendrowski, S., MacArthur, W., and Hanna, P. (2004) *Bacillus anthracis* requires siderophore biosynthesis for growth in macrophages and mouse virulence. *Mol. Microbiol. 51*, 407−417.

(12) Wilson, M. K., Abergel, R. J., Raymond, K. N., Arceneaux, J. E., and Byers, B. R. (2006) Siderophores of *Bacillus anthracis*, *Bacillus cereus*, and *Bacillus thuringiensis*. *Biochem. Biophys. Res. Commun. 348*, 320−325.

(13) Brickman, T. J., and McIntosh, M. A. (1992) Overexpression and purification of ferric enterobactin esterase from *Escherichia coli*. Demonstration of enzymatic hydrolysis of enterobactin and its iron complex. *J. Biol. Chem. 267*, 12350−12355.

(14) Lin, H., Fischbach, M. A., Liu, D. R., and Walsh, C. T. (2005) *In vitro* characterization of salmochelin and enterobactin trilactone hydrolases IroD, IroE, and Fes. *J. Am. Chem. Soc. 127*, 11075−11084.

(15) Zhu, M., Valdebenito, M., Winkelmann, G., and Hantke, K. (2005) Functions of the siderophore esterases IroD and IroE in iron-salmochelin utilization. *Microbiology 151*, 2363−2372.

(16) Miethke, M., Klotz, O., Linne, U., May, J. J., Beckering, C. L., and Marahiel, M. A. (2006) Ferri-bacillibactin uptake and hydrolysis in *Bacillus subtilis*. *Mol. Microbiol. 61*, 1413−1427.

(17) Abergel, R. J., Zawadzka, A. M., Hoette, T. M., and Raymond, K. N. (2009) Enzymatic hydrolysis of trilactone siderophores: Where chiral recognition occurs in enterobactin and bacillibactin iron transport. *J. Am. Chem. Soc. 131*, 12682−12692.

(18) Dertz, E. A., and Raymond, K. N. (2004) Biochemical and physical properties of siderophores. In *Iron transport in bacteria* (Crosa, J. H., Mey, A. R., and Payne, S. M., Eds.) pp 3−17, American Society for Microbiology Press, Washington, DC.

(19) Jewett, S. L., Eggling, S., and Geller, L. (1997) Novel method to examine the formation of unstable 2:1 and 3:1 complexes of catecholamines and iron(III). *J. Inorg. Biochem. 66*, 165−173.

(20) Schröder, I., Johnson, E., and de Vries, S. (2003) Microbial ferric iron reductases. *FEMS Microbiol. Rev. 27*, 427−447.

(21) Winkelmann, G., and Drechsel, H. (1997) Microbial Siderophores. In *Products of Secondary Metabolism* (Kleinkauf, H., and von Döhren, H., Eds.) pp 200−246, Wiley-VCH, Weinheim, Germany.

(22) Butterton, J. R., and Calderwood, S. B. (1994) Identification, cloning, and sequencing of a gene required for ferric vibriobactin utilization by *Vibrio cholerae*. *J. Bacteriol. 176*, 5631−5638.

(23) Joint Center for Structural Genomics (2006) Crystal structure of siderophore-interacting protein (SPUTCN32_0076) from *Shewanella putrefaciens* CN-32 at 2.20 Å resolution. RCSB Protein Data Bank, entry 2GPJ.

(24) Bamford, V. A., Armour, M., Mitchell, S. A., Cartron, M., Andrews, S. C., and Watson, K. A. (2008) Preliminary X-ray diffraction analysis of YqjH from *Escherichia coli*: A putative cytoplasmic ferri-siderophore reductase. *Acta Crystallogr. F64*, 792−796.
(25) McHugh, J. P., Rodriguez-Quinones, F., Abdul-Tehrani, H., Svistunenko, D. A., Poole, R. K., Cooper, C. E., and Andrews, S. C. (2003) Global iron-dependent gene regulation in *Escherichia coli*. A new mechanism for iron homeostasis. *J. Biol. Chem. 278*, 29478−29486.
(26) Wang, S., Wu, Y., and Outten, F. W. (2011) Fur and the novel regulator YqjI control transcription of the ferric reductase gene *yqjH* in *Escherichia coli*. *J. Bacteriol. 193*, 563−574.
(27) Miethke, M., Pierik, A. J., Peuckert, F., Seubert, A., and Marahiel, M. A. (2011) Identification and characterization of a novel-type ferric siderophore reductase from a Gram-positive extremophile. *J. Biol. Chem. 286*, 2245−2260.
(28) Sambrook, J., Fritsch, E. F., and Maniatis, T. (1989) *Molecular Cloning: A Laboratory Manual*, Cold Spring Harbor Laboratory Press, Plainview, NY.
(29) Bradford, M. M. (1976) A rapid and sensitive method for the quantitation of microgram quantities of protein utilizing the principle of protein-dye binding. *Anal. Biochem. 72*, 248−254.
(30) Fischbach, M. A., Lin, H., Liu, D. R., and Walsh, C. T. (2005) *In vitro* characterization of IroB, a pathogen-associated C-glycosyltransferase. *Proc. Natl. Acad. Sci. U.S.A. 102*, 571−576.
(31) Tor, Y., Libman, J., Shanzer, A., Felder, C. E., and Lifson, S. (1992) Chiral siderophore analogs: Enterobactin. *J. Am. Chem. Soc. 114*, 6661−6671.
(32) Garrett, T. M., Mcmurry, T. J., Hosseini, M. W., Reyes, Z. E., Hahn, F. E., and Raymond, K. N. (1991) Synthesis and characterization of macrobicyclic iron(III) sequestering agents. *J. Am. Chem. Soc. 113*, 2965−2977.
(33) Rastetter, W. H., Erickson, T. J., and Venuti, M. C. (1981) Synthesis of iron chelators. Enterobactin, enantioenterobactin, and a chiral analog. *J. Org. Chem. 46*, 3579−3590.
(34) Macheroux, P. (1999) UV-visible spectroscopy as a tool to study flavoproteins. In *Methods in Molecular Biology: Flavoprotein Protocols* (Chapman, S. K., and Read, G. A., Eds.) Vol. *131*, pp 1−7, Humana Press Inc., Totowa, NJ.
(35) Baba, T., Ara, T., Hasegawa, M., Takai, Y., Okumura, Y., Baba, M., Datsenko, K. A., Tomita, M., Wanner, B. L., and Mori, H. (2006) Construction of *Escherichia coli* K-12 in-frame, single-gene knockout mutants: The Keio collection. *Mol. Syst. Biol. 2*, 2006.0008.
(36) Wach, A. (1996) PCR-synthesis of marker cassettes with long flanking homology regions for gene disruptions in *S. cerevisiae*. *Yeast 12*, 259−265.
(37) Datsenko, K. A., and Wanner, B. L. (2000) One-step inactivation of chromosomal genes in *Escherichia coli* K-12 using PCR products. *Proc. Natl. Acad. Sci. U.S.A. 97*, 6640−6645.
(38) Valdebenito, M., Crumbliss, A. L., Winkelmann, G., and Hantke, K. (2006) Environmental factors influence the production of enterobactin, salmochelin, aerobactin, and yersiniabactin in *Escherichia coli* strain Nissle 1917. *Int. J. Med. Microbiol. 296*, 513−520.
(39) Cole, C., Barber, J. D., and Barton, G. J. (2008) The Jpred 3 secondary structure prediction server. *Nucleic Acids Res. 36*, W197−W201.
(40) Ouali, M., and King, R. D. (2000) Cascaded multiple classifiers for secondary structure prediction. *Protein Sci. 9*, 1162−1176.
(41) Lambert, C., Leonard, N., De Bolle, X., and Depiereux, E. (2002) ESyPred3D: Prediction of proteins 3D structures. *Bioinformatics 18*, 1250−1256.
(42) Goetz, D. H., Holmes, M. A., Borregaard, N., Bluhm, M. E., Raymond, K. N., and Strong, R. K. (2002) The neutrophil lipocalin NGAL is a bacteriostatic agent that interferes with siderophore-mediated iron acquisition. *Mol. Cell 10*, 1033−1043.
(43) Müller, A., Wilkinson, A. J., Wilson, K. S., and Duhme-Klair, A. K. (2006) An $[\{Fe(mecam)\}_2]^{6-}$ bridge in the crystal structure of a ferric enterobactin binding protein. *Angew. Chem., Int. Ed. 45*, 5132−5136.
(44) Peuckert, F., Miethke, M., Albrecht, A. G., Essen, L. O., and Marahiel, M. A. (2009) Structural basis and stereochemistry of triscatecholate siderophore binding by FeuA. *Angew. Chem., Int. Ed. 48*, 7924−7927.
(45) Murataliev, M. B., Klein, M., Fulco, A., and Feyereisen, R. (1997) Functional interactions in cytochrome P450BM3: Flavin semiquinone intermediates, role of NADP(H), and mechanism of electron transfer by the flavoprotein domain. *Biochemistry 36*, 8401−8412.
(46) Neilands, J. B. (1995) Siderophores: Structure and function of microbial iron transport compounds. *J. Biol. Chem. 270*, 26723−26726.
(47) Crosa, J. H., and Walsh, C. T. (2002) Genetics and assembly line enzymology of siderophore biosynthesis in bacteria. *Microbiol. Mol. Biol. Rev. 66*, 223−249.
(48) Pasek, J., Buechler, R., Albrecht, R., Boland, W., and Zeth, K. (2011) Structure and mechanism of iron translocation by a DPS protein from *Microbacterium arborescens*. *J. Biol. Chem. 286*, 34872−34882.
(49) Hantke, K. (2001) Iron and metal regulation in bacteria. *Curr. Opin. Microbiol. 4*, 172−177.
(50) Fontecave, M., Choudens, S. O., Py, B., and Barras, F. (2005) Mechanisms of iron-sulfur cluster assembly: The SUF machinery. *J. Biol. Inorg. Chem. 10*, 713−721.
(51) Lecerof, D., Fodje, M., Hansson, A., Hansson, M., and Al-Karadaghi, S. (2000) Structural and mechanistic basis of porphyrin metallation by ferrochelatase. *J. Mol. Biol. 297*, 221−232.
(52) Carrillo, N., and Ceccarelli, E. A. (2003) Open questions in ferredoxin-$NADP^+$ reductase catalytic mechanism. *Eur. J. Biochem. 270*, 1900−1915.
(53) Forti, G., and Sturani, E. (1968) On the structure and function of reduced nicotinamide adenine dinucleotide phosphate-cytochrome *f* reductase of spinach chloroplasts. *Eur. J. Biochem. 3*, 461−472.
(54) Sem, D. S., and Kasper, C. B. (1994) Kinetic mechanism for the model reaction of NADPH-cytochrome P450 oxidoreductase with cytochrome *c*. *Biochemistry 33*, 12012−12021.
(55) Kirchner, U., Westphal, A. H., Muller, R., and van Berkel, W. J. (2003) Phenol hydroxylase from *Bacillus thermoglucosidasius* A7, a two-protein component monooxygenase with a dual role for FAD. *J. Biol. Chem. 278*, 47545−47553.
(56) Li, R., Bianchet, M. A., Talalay, P., and Amzel, L. M. (1995) The three-dimensional structure of NAD(P)H:quinone reductase, a flavoprotein involved in cancer chemoprotection and chemotherapy: Mechanism of the two-electron reduction. *Proc. Natl. Acad. Sci. U.S.A. 92*, 8846−8850.
(57) Raymond, K. N., Müller, G., and Matzanke, B. F. (1984) Complexation of iron by siderophores. A review of their solution and structural chemistry and biological function. *Top. Curr. Chem. 123*, 49−102.
(58) Matzanke, B. F., Ecker, D. J., Yang, T. S., Huynh, B. H., Muller, G., and Raymond, K. N. (1986) *Escherichia coli* iron enterobactin uptake monitored by Mossbauer spectroscopy. *J. Bacteriol. 167*, 674−680.
(59) Ecker, D. J., Matzanke, B. F., and Raymond, K. N. (1986) Recognition and transport of ferric enterobactin in *Escherichia coli*. *J. Bacteriol. 167*, 666−673.